Title
The central clock suffices to drive the majority of circulatory metabolic rhythms

Journal
Science Advances, 8(26)

ISSN
2375-2548

Authors
Petrus, Paul
Smith, Jacob G
Koronowski, Kevin B
et al.

Publication Date
2022-07-01

DOI
10.1126/sciadv.abo2896

PHYSIOLOGY

The central clock suffices to drive the majority of circulatory metabolic rhythms

Paul Petrus[1]*, Jacob G. Smith[1,2], Kevin B. Koronowski[1], Siwei Chen[3,4], Tomoki Sato[1,5], Carolina M. Greco[1,6], Thomas Mortimer[7], Patrick-Simon Welz[8], Valentina M. Zinna[7], Kohei Shimaji[1], Marlene Cervantes[1], Daniela Punzo[9], Pierre Baldi[3,4], Pura Muñoz-Cánoves[2,10,11]*†, Paolo Sassone-Corsi[1]†, Salvador Aznar Benitah[7,12]*†

Life on Earth anticipates recurring 24-hour environmental cycles via genetically encoded molecular clocks active in all mammalian organs. Communication between these clocks controls circadian homeostasis. Intertissue communication is mediated, in part, by temporal coordination of metabolism. Here, we characterize the extent to which clocks in different organs control systemic metabolic rhythms, an area that remains largely unexplored. We analyzed the metabolome of serum from mice with tissue-specific expression of the clock gene *Bmal1*. Having functional hepatic and muscle clocks can only drive a minority (13%) of systemic metabolic rhythms. Conversely, limiting *Bmal1* expression to the central pacemaker in the brain restores rhythms to 57% of circulatory metabolites. Rhythmic feeding imposed on clockless mice resulted in a similar rescue, indicating that the central clock mainly regulates metabolic rhythms via behavior. These findings explicate the circadian communication between tissues and highlight the importance of the central clock in governing those signals.

INTRODUCTION

Throughout evolution, the Earth has spun around its own axis with a 24-hour cycle. Thus, life has adapted to the reoccurring environmental fluctuations that accompany Earth's rotation with a genetically encoded molecular clock, henceforth the core clock machinery (*1*). These clocks exist in every organ in the mammalian body and are believed to cooperate to control circadian homeostasis (*2*). A way of interorgan communication is via metabolic fluctuations, which is believed to function similar to an economic system taking the supply and demand of various tissues into consideration (*3*, *4*). Systemic metabolic homeostasis is temporally coordinated between tissues and is perturbed when challenged with a high-fat diet (*5*). Nevertheless, the contribution of specific tissue clocks in regulating systemic metabolic rhythms remains a virtually unexplored field.

To address the degree to which specific-tissue clocks can regulate systemic metabolism, we first analyzed the role of local clocks in driving the strong temporal metabolic coherence that exists among serum, liver, and muscle (*5*). Metabolic rhythms are intimately linked with the core clock machinery, which comprises a transcriptional-translational feedback loop: The transcription factors BMAL1 (brain and muscle ARNT-like 1) and CLOCK (circadian locomotor output cycles kaput) heterodimerize and bind to E-box elements, thereby transcribing an array of genes that includes their own repressors *Period1-3* and *Cryptochorme1-2* (*6*, *7*). This feedback loop takes about 24 hours to complete and integrates metabolic input and output to control circadian homeostasis (*8*). To determine the metabolic output of tissue specific clocks, we used our previously generated conditional gene trap approach (*9*, *10*), in which tissue-specific expression of *Bmal1* is achieved through Cre-mediated excision of a stop-flox (FL) cassette between exons 5 and 6 of *Bmal1* in mice. Expression of Cre recombinase under the *Alfp* or *Hsa* promotor results in selective *Bmal1* expression in the liver (liver-RE) (*9*) or skeletal muscle (muscle-RE) (*11*), respectively. Furthermore, mice without *Bmal1*-stop-FL are wild-type (WT) for *Bmal1* (e.g., it is expressed in all tissues), while Cre-negative *Bmal1*-stop-FL mice are knockout (KO) for *Bmal1* organism wide.

[1]Center for Epigenetics and Metabolism, U1233 INSERM, Department of Biological Chemistry, University of California, Irvine, Irvine, CA 92697, USA. [2]Department of Experimental and Health Sciences, Pompeu Fabra University (UPF), CIBER on Neurodegenerative Diseases (CIBERNED), E-08003 Barcelona, Spain. [3]Department of Computer Science, University of California, Irvine, Irvine, CA 92697, USA. [4]Institute for Genomics and Bioinformatics, University of California, Irvine, Irvine, CA 92697, USA. [5]Laboratory of Nutritional Biochemistry, Graduate School of Nutritional and Environmental Sciences, University of Shizuoka, Shizuoka 422-8526, Japan. [6]Department of Biomedical Sciences, Humanitas University and Humanitas Research Hospital IRCCS, Via Manzoni 56, 20089 Rozzano (Milan), Italy. [7]Institute for Research in Biomedicine (IRB Barcelona), The Barcelona Institute of Science and Technology (BIST), 08028 Barcelona, Spain. [8]Hospital del Mar Medical Research Institute (IMIM), Cancer Research Programme, 08003 Barcelona, Spain. [9]School of Medicine, Department of Microbiology and Molecular Genetics, INSERMU1233, Center for Epigenetics and Metabolism, University of California, Irvine, Irvine, CA 92697, USA. [10]ICREA, Catalan Institution for Research and Advanced Studies, Barcelona, Spain. [11]Spanish National Center on Cardiovascular Research (CNIC), E-28029 Madrid, Spain. [12]Catalan Institution for Research and Advanced Studies (ICREA), 08010 Barcelona, Spain.
*Corresponding author. Email: salvador.aznar-benitah@irbbarcelona.org (S.A.-B.); pura.munoz@upf.edu (P.M.-C.); ppetrus@uci.edu (P.P.)
†These authors contributed equally to this work.

RESULTS AND DISCUSSION

Mice were euthanized every 4 hours during a 24-hour diurnal cycle, and serum was collected from all genotypes. The serum samples were analyzed by global metabolomics using liquid chromatography–mass spectrometry (LC/MS). In WT mice, 25% (217/868) of detected circulating metabolites displayed significant circadian oscillations [table S1; JTK_CYCLE (Jonckheere-Terpstra-Kendall cycle) (*12*); $P < 0.05$]. *Bmal1*-KO mice lost rhythmicity of all metabolites observed for WT except for cysteine-*S*-sulfate (Fig. 1A), confirming that *Bmal1* expression is crucial for oscillations in circulatory metabolites. Reconstitution of the hepatic clock (liver-RE) or muscle clock (muscle-RE mice) restored a unique set of metabolites by each tissue; strikingly, however, these metabolites only comprised ~13% of the WT oscillating metabolome (Fig. 1B). These data suggest that local peripheral clocks in isolation are insufficient to drive the majority of the circadian metabolic output into circulation. Notably, similar to

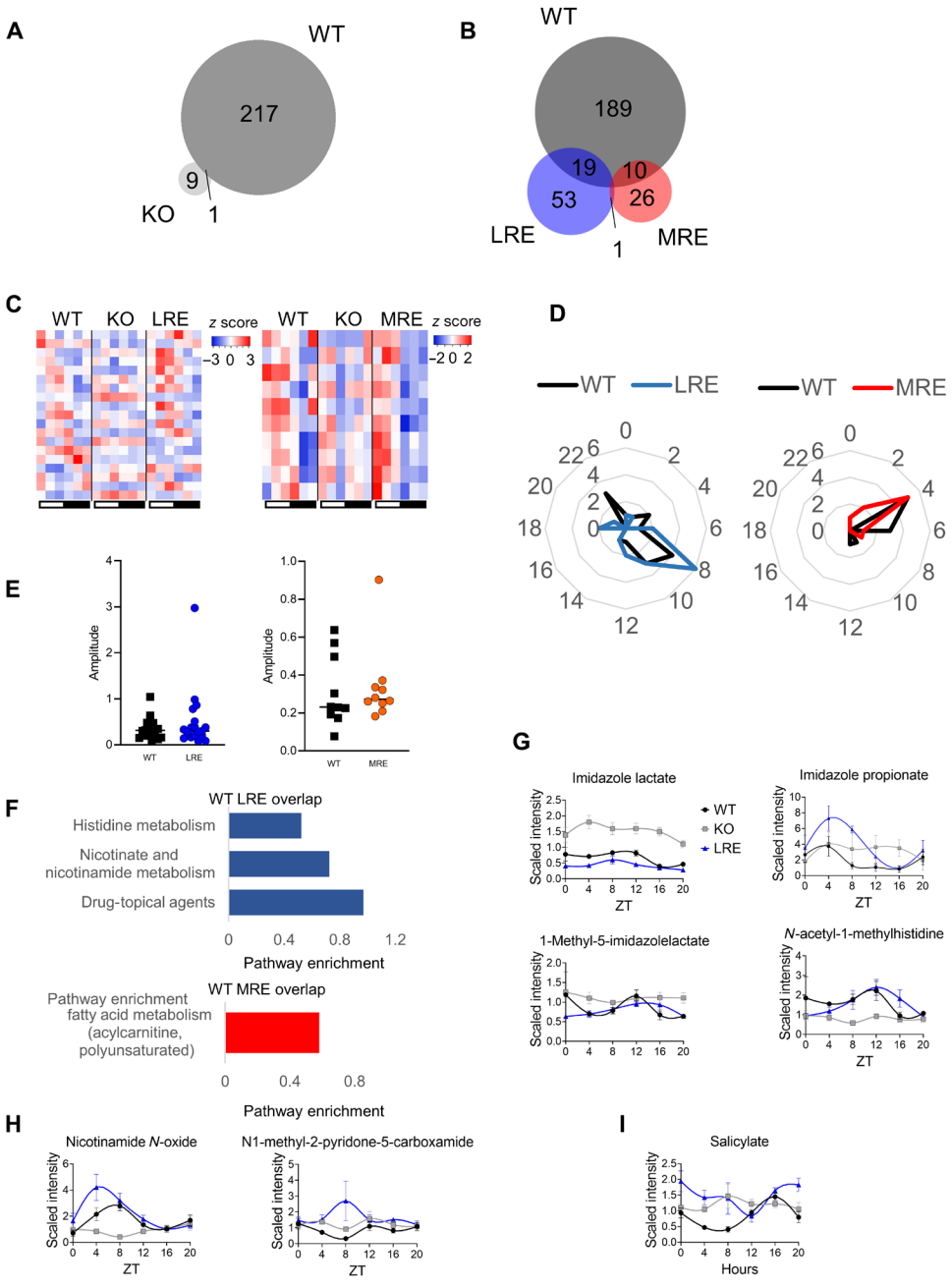

Fig. 1. The hepatic and muscular clocks are mediating a minority of rhythmic metabolic rhythms in the circulation. (**A**) Venn diagram representing the overlap of significantly oscillating (JTK, $P < 0.05$) serum metabolites between wild-type (WT) and *Bmal1* knockout (KO) mice. (**B**) Venn diagram representing the overlap between of significantly oscillating (JTK, $P < 0.05$) serum metabolites in WT, *Bmal1* liver-reconstituted (LRE), and *Bmal1* muscle-reconstituted (MRE) mice. (**C**) Heatmaps representing the oscillating metabolites overlapping between WT and LRE (left heatmap) or WT and MRE (right heatmap). (**D**) Radar plots illustrating the phase of the metabolic oscillations of the overlapping metabolites between WT and LRE (left radar plot) or WT and MRE (right radar plot). (**E**) Graphs displaying the amplitudes of the overlapping metabolites between WT and LRE (left graph) or WT and MRE (right graph). (**F**) Pathway enrichment of overlapping metabolites. Significantly oscillating metabolites withing the (**G**) histidine, (**H**) nicotinate and nicotinamide, and (**I**) drug-topical agents presented in graphs. All analyses were performed using $n = 4$ mice.

Bmal1-KO mice, liver-RE and muscle-RE mice lacked detectable feeding-fasting cycles, and daily differences in locomotor activity were markedly reduced as compared to WT (*9*, *11*). Nevertheless, the oscillating metabolites common between WT and liver-RE or muscle-RE mice displayed a similar circadian pattern as in WT mice (Fig. 1B), with aligned phases (Fig. 1D) and amplitudes (Fig. 1E). These metabolites comprised intermediates in the histidine, nicotinamide, and topical agent pathways for the liver clock and polyunsaturated acylcarnitine for the muscle clock (Fig. 1F). Notably, regulation of nicotinamide metabolism provides a link to the clock system: Expression of *Nampt* is controlled via the core clock machinery and generates nicotinamide adenine dinucleotide through the salvage pathway

(*13*), which feedback to regulate the clock machinery via sirtuin 1 (SIRT1) activity (*14*). In addition, histidine metabolism has been linked to circadian rhythms in the brain (*15*), presenting a potential role of the hepatic clock in regulating central functions. However, the autonomous liver clock is unlikely to regulate behavioral rhythms, as liver-RE mice display arrhythmic behaviors of feeding and locomotor activity (*9*). Furthermore, the muscle clock is necessary for local lipid metabolism, including for long-chain polyunsaturated fatty acid metabolism (*16*); data from the muscle-RE serum demonstrated partial sufficiency of this metabolic pathway. In summary, autonomous liver and muscle clocks in isolation are sufficient to drive only a small number of metabolic rhythms in circulation, revealing that the majority of circulatory metabolites are dependent on other tissue clocks or communication between tissue clocks.

Metabolic rhythms require substrates via food intake or from stores within the body (*4*). Thus, rhythmic feeding behavior is likely a key determinant of systemic metabolic oscillations. Behavioral rhythms are controlled by the central clock of the suprachiasmatic nucleus (SCN) (*17*). The *Syt10* gene is highly expressed in the central circadian pacemaker located within the SCN, along with other brain regions (fig. S1A) (*18*, *19*). Knocking out *Bmal1* in *Syt10*-expressing neurons results in arrhythmic behavior when the mice are placed in constant darkness (*19*). To study the degree to which centrally expressed *Bmal1* is sufficient for generating systemic metabolic rhythms, we crossed the stop-FL mice with mice expressing the Cre recombinase under the control of the *Syt10* promotor (hereafter referred to as brain-RE). BMAL1 was successfully expressed in the brains of brain-RE mice, including within the SCN, but also in other brain regions such as the prefrontal cortex and hippocampus. BMAL1 was not expressed in peripheral tissues of the brain-RE mice (fig. S1, B to F).

To assess whether BMAL1 expression in Syt10 neurons restored behavioral rhythms, we next analyzed locomotor activity, metabolism, and feeding behavior for brain-RE mice as compared to WT or KO mice. The body weight of brain-RE mice was partially rescued in relation to KO mice, and total activity, food intake, and adiposity displayed a trend toward a rescue (fig. S2A). Circadian rhythms of behavior and metabolism were partially restored in the brain-RE mice and maintained rhythmicity in constant darkness (fig. S2, B to D). Partial restoration implies that clocks in other cell types of the brain, and potentially peripheral clocks as well, are required for full robustness of behavioral rhythms. The lower amplitude of locomotor activity and feeding is likely the cause of lost rhythmicity of energy expenditure and respiratory exchange ratio. Despite partially rescued behavior, brain-RE mice displayed a remarkable number of metabolite oscillations in serum, with a 57% overlap with those in WT (e.g., of the 223 metabolites in WT mice, 124 were found in brain-RE) (Fig. 2A), suggesting that the central clock governs processes that define the majority of systemic metabolic rhythms. Oscillating metabolites common to WT and brain-RE mice exhibited similar phases; however, most daytime metabolites peaked with a 4-hour delay in the brain-RE as compared to WT mice (Fig. 2, B and C). Strikingly, in brain-RE mice, 174 (of 298) metabolites gained de novo oscillation (Fig. 2A), and the amplitudes of commonly oscillating metabolites were significantly reduced, as compared to WT mice (Fig. 2D). These results suggest that peripheral clocks (and/or other brain clocks) are able to suppress aberrantly oscillating metabolites mediated by the central clock while also modulating the amplitudes and phase of others.

The metabolic classes that displayed increased amplitudes in brain-RE mice included nucleotide- and energy-related metabolites, as well as partially characterized molecules (Fig. 2E). In contrast, carbohydrates displayed mainly a reduced amplitude in brain-RE mice (Fig. 2E). Although the hepatic and muscle clocks alone cannot drive systemic oscillations of carbohydrate metabolites, they are necessary to buffer these rhythms (*20*, *21*). The commonly oscillating metabolites were enriched for various acylcarnitines and the urea cycle, along with metabolites in the drug-topical agent class (Fig. 2F and fig. S3). Ureagenesis is controlled by the core clock protein CLOCK (*22*), suggesting that the components of the clock machinery may continue to control circadian metabolic homeostasis possibly via other unknown feedback loops. The uniquely oscillating metabolites in WT or brain-RE mice were enriched for several fatty acid metabolic classes or sphingomyelin metabolism, respectively (fig. S4, A and B). Most oscillating metabolites belonged to the amino acid, lipid, and xenobiotic metabolic classes; oscillation patterns of amino acids and xenobiotics were similar between WT and brain-RE, while that of lipids peaked with a 4-hour delay in brain-RE mice (Fig. 2G). Together, these data suggest that the central clock is sufficient to drive most circadian circulating metabolic rhythms, yet phase and amplitude often requiring additional regulation by other clocks.

We next investigated to what degree the central clock suffices in regulating transcriptional oscillations of the periphery in the absence of peripheral clocks. We thus studied the hepatic rhythmic transcriptome from brain-RE mice by performing RNA sequencing (RNA-seq) over a 24-hour period (table S2). Of the 3392 oscillating genes in WT livers, 923 oscillated in brain-RE livers (Fig. 3A). Thus, the central clock is sufficient for driving ~27% of the hepatic transcriptome, which is higher than the ~13% driven by the local autonomous liver clock (*9*). The liver-RE mice displayed a higher recovery (~41%) of the circadian liver transcriptome once feeding rhythms were introduced (*23*), suggesting that regulation both by the local clock and by feeding rhythms were additive rather than redundant (27% + 13% = 41%). The transcription phases were distributed throughout the day in WT livers, while most hepatic mRNAs peak at ZT6 (zeitgeber time 6) and ZT18 in brain-RE mice (Fig. 3B, C), possibly in direct response to the feeding-fasting cycles. In line with the serum metabolite rhythms, the amplitude of hepatic transcripts was higher in brain-RE than WT mice (Fig. 3D). The commonly oscillating transcripts were enriched for genes involved in the peroxisome pathway and the circadian clock system (Fig. 3E and fig. S5, A and B). The former is in agreement with the oscillations observed in the acylcarnitine pathway (Fig. 2F), suggesting that fatty acid beta oxidation in peroxisomes, which results in excessive acylcarnitine, is under the central circadian control. Notably, oscillations of the circadian genes *Per1* and *Per2* were similar in WT and brain-RE livers, suggesting that their transcriptional control can be uncoupled from hepatic *Bmal1* (fig. S5A) and is likely driven by systemic signals (*24*). This implies that the central clock can mediate peripheral circadian rhythms, through circadian clock components but independently from the core clock machinery. PER2 (period circadian regulator 2) controls lipid metabolism via the adipogenic transcription factor peroxisome proliferator–activated receptor γ (*25*), which presents a potential mechanism explaining the recovered oscillations of systemic metabolism in the brain-RE mice. The brain clock–driven changes in the hepatic chromatin architecture are an intriguing question that ought to be investigated in future studies. Furthermore, 2425 genes were only rhythmic in WT mice (Fig. 3A), including the ones involved in vascular endothelial growth factor A signaling and hypoxia-inducible factor–1α, in the interferon-γ pathway and the

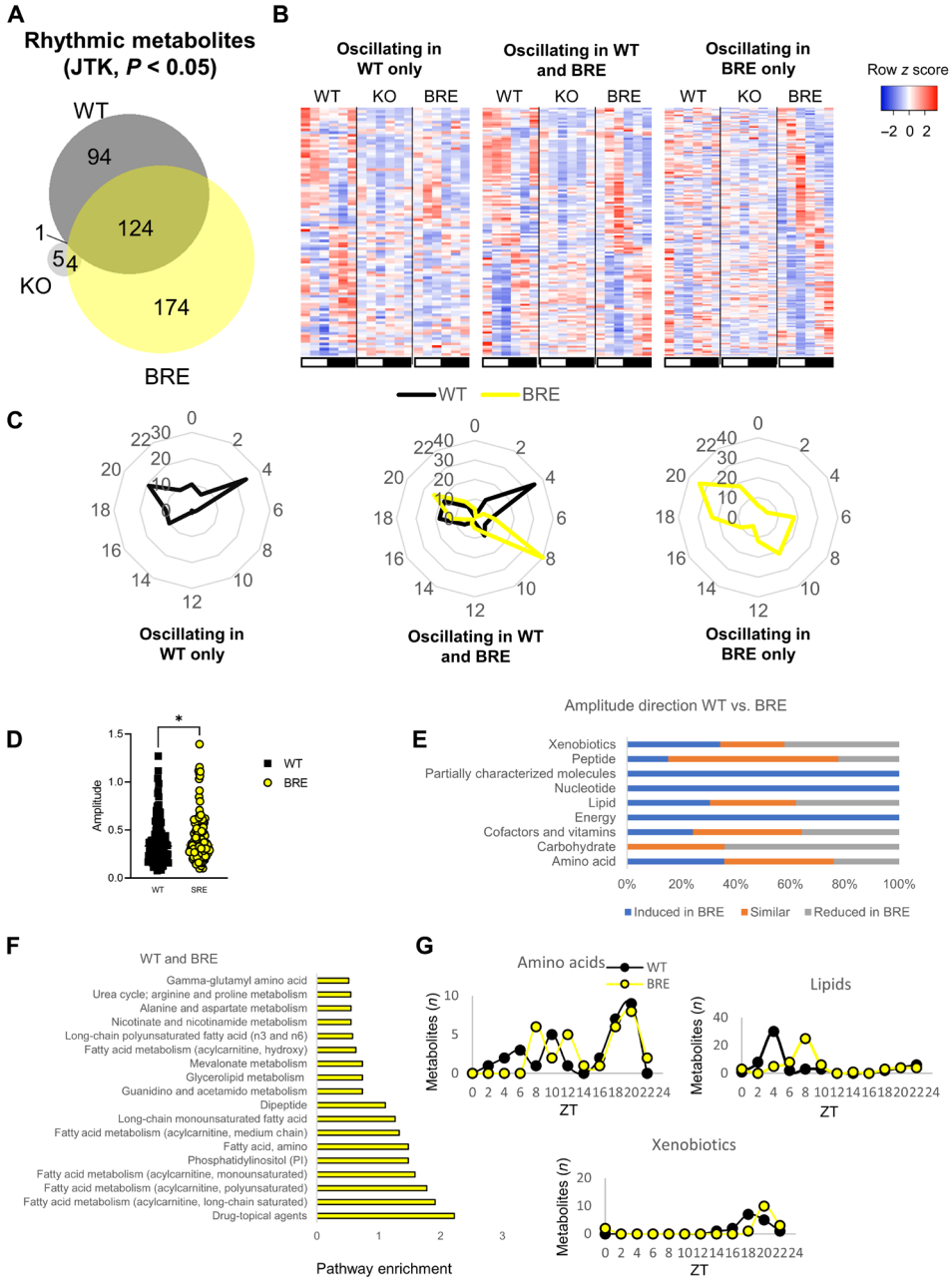

Fig. 2. The majority of rhythmic regulation of circulating metabolites is driven by the central clock. (**A**) Venn diagram representing the overlap of significantly oscillating (JTK, $P < 0.05$) serum metabolites between WT, *Bmal1* KO mice, and *Bmal1* brain-RE (BRE). (**B**) Heatmaps representing the oscillating metabolites in WT only (left heatmap), overlapping between WT and BRE (middle heatmap) and in BRE only (right heatmap). (**C**) Radar plots illustrating the phase of the metabolic oscillations in WT only (left radar plot), overlapping between WT and BRE (middle radar plot), and in BRE only (right radar plot). (**D**) Graph displaying the amplitudes of the overlapping metabolites between WT and BRE. Significant difference was assessed by paired *t* test. (**E**) The change in amplitude within each pathway in BRE mice in relation to WT. (**F**) Pathway enrichment of oscillating metabolites overlapping between WT and BRE. (**G**) Phase of metabolites in the major oscillating metabolic classes. *$P < 0.05$. All analyses were performed using $n = 4$ mice.

methionine cycle (figs. S6A and S7, A and B). These pathways have all been linked to the clock system (*26*–*28*) and require peripheral clocks to maintain circadian homeostasis. De novo oscillating transcripts in the brain-RE livers were strongly enriched for genes in the branched-chain amino acid pathway (figs. S6B and S8); however, oscillations in circulating metabolites in this pathway were not enriched in brain-RE mice (Fig. 2F).

Glucose metabolism is controlled by the circadian system, and systemic glucose homeostasis requires clocks in multiple organs (*4*), but the degree to which each clock suffices is unclear. We observed a rescue of acylcarnitine oscillations in brain-RE mice, which may potentially play a role in linking fatty acid oxidation and glucose homeostasis (*29*). Hence, we hypothesized that the brain clock regulates glucose homeostasis, independent of peripheral clocks. Thus,

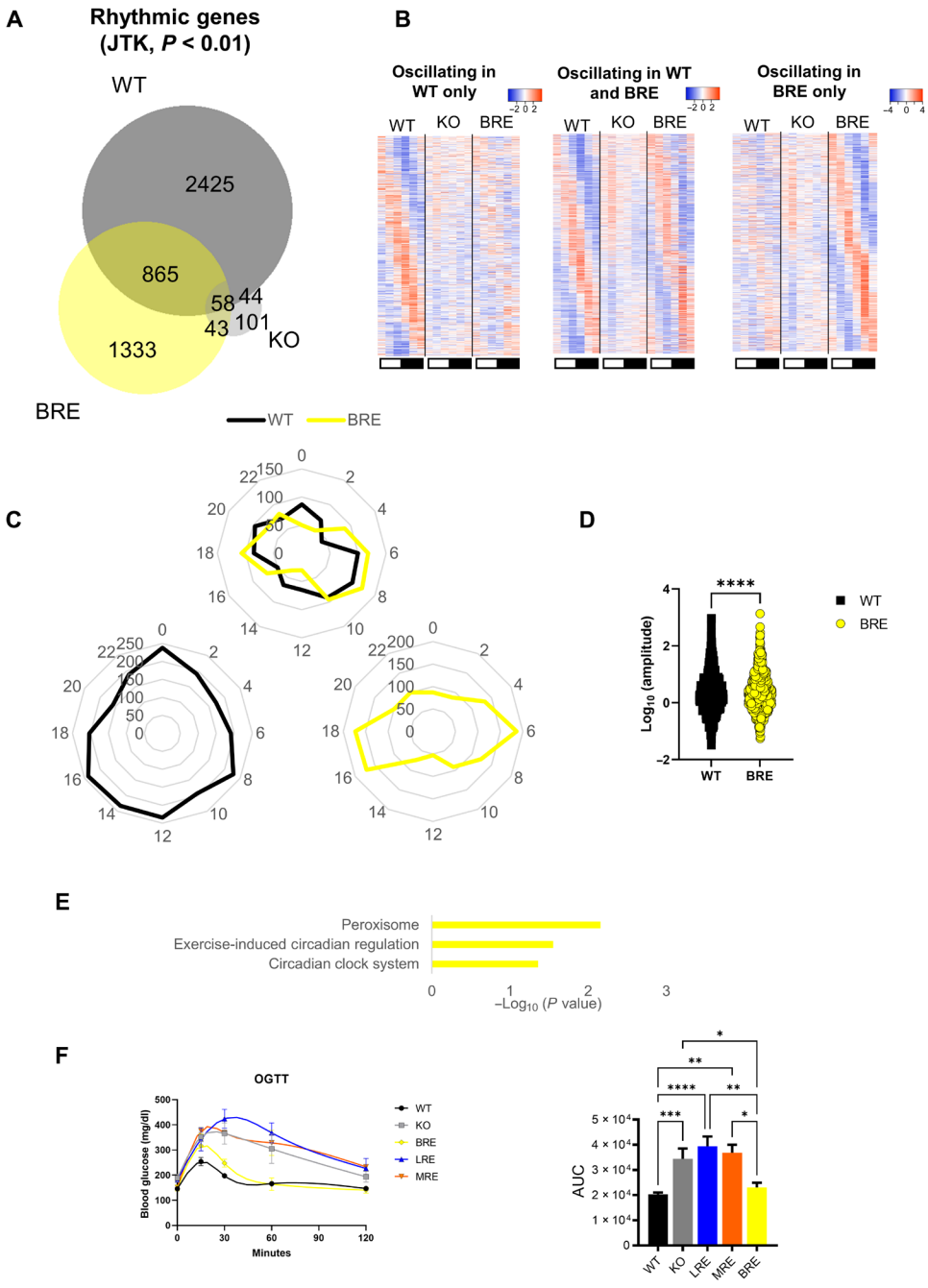

Fig. 3. The central clock is sufficient to drive circadian rhythms of hepatic transcription and to restore glucose tolerance. (**A**) Venn diagram representing the overlap of significantly oscillating (JTK, $P < 0.01$) liver transcripts between WT, *Bmal1* KO mice, and *Bmal1* BRE. (**B**) Heatmaps representing the oscillating transcripts in WT only (left heatmap), overlapping between WT and BRE (middle heatmap), and in BRE only (right heatmap). (**C**) Radar plots illustrating the phase of transcriptional oscillations in WT only (bottom left radar plot), overlapping between WT and BRE (top radar plot), and in BRE only (bottom right radar plot). (**D**) Graph displaying the amplitudes of the overlapping oscillating transcripts between WT and BRE. Significant difference was assessed by paired *t* test. (**E**) Pathway enrichment of oscillating transcripts overlapping between WT and BRE mice. (**F**) Oral glucose tolerance test (OGTT) and the calculated area under the curve (AUC) in all genotypes presented in the study. Significant differences were analyzed by a one-way analysis of variance (ANOVA) followed by the Fisher's least significant difference post hoc test. *$P < 0.05$, **$P < 0.01$, ***$P < 0.001$, and ****$P < 0.0001$. All analyses were performed using at least $n = 3$ mice.

we performed oral glucose tolerance tests in all RE genotypes presented herein. Bmal1-KO mice displayed a poor glucose tolerance, and this was not improved by reconstituting either the liver or muscle clock alone (Fig. 3F). The glucose intolerance in these mice is likely not time dependent as these effects are also observed in the rest phase, at ZT4 (*11*). In contrast and in accordance with our hypothesis, brain-RE mice had a notably improved glucose tolerance (Fig. 3F). This finding that the central clock suffices for glucose homeostasis

complements a recent work, showing that it is necessary for glucose homeostasis (*30*), and is in line with a previous work, showing that time-restricted feeding prevents glucose intolerance in clock-disrupted mice (*31*). Together, these results underscore the importance of central processes in regulating glucose homeostasis and expand on the knowledge linking shift work to diabetes (*32*).

We next aimed to characterize the processes by which the central clock regulates systemic metabolism. We hypothesized that metabolic oscillations are driven by rhythmic feeding behavior, a process restored in the brain-RE (BRE) mice (fig. S2C). First, ad hoc analyses were performed on the data from our published study (*23*), which assessed hepatic metabolite and transcript rhythms in KO mice

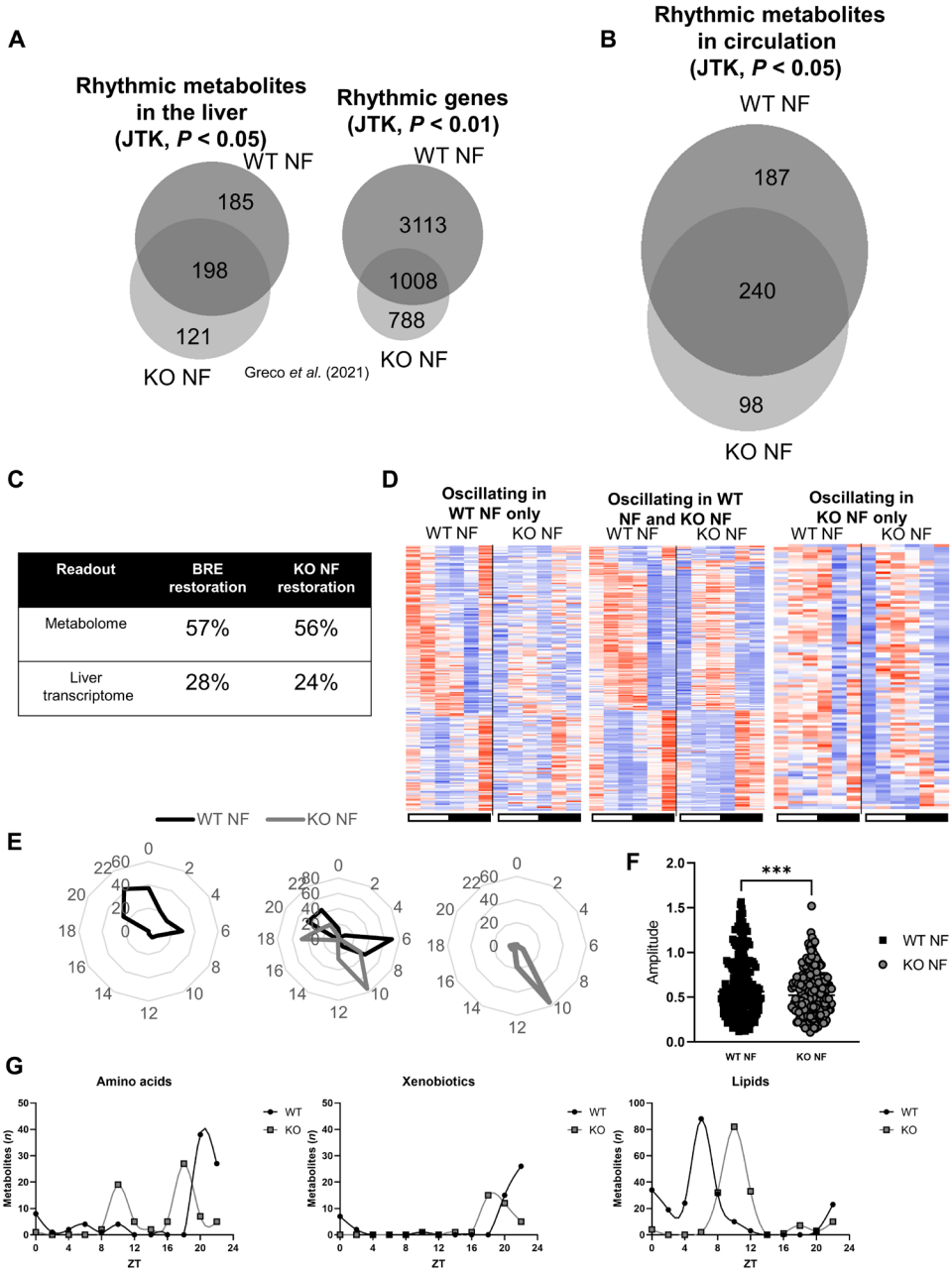

Fig. 4. Serum metabolite oscillations are mainly driven by feeding rhythms. (**A**) Venn diagram representing the overlap of significantly oscillating liver metabolites (JTK, $P < 0.05$) and transcripts (JTK, $P < 0.01$) between WT and *Bmal1* KO mice subjected to NF. These are ad hoc analyses by publicly available datasets from our previous paper. (**B**) Venn diagram representing the overlap of significantly oscillating serum metabolites (JTK, $P < 0.05$) between WT and *Bmal1* KO mice subjected to NF. (**C**) Comparison of proportion of metabolites and transcripts reconstituted upon reintroducing the clock in the SCN or NF. (**D**) Heatmaps representing the oscillating transcripts in WT NF only (left heatmap), overlapping between WT NF and KO NF (middle heatmap), and in KO NF only (right heatmap). (**E**) Radar plots illustrating the phase of circulatory metabolic oscillations in WT NF only (left radar plot), overlapping between WT NF and KO NF (middle radar plot), and in KO NF only (right radar plot). (**F**) Graph displaying the amplitudes of the overlapping oscillating metabolites between WT NF and KO NF. Significant difference was assessed by paired *t* test. (**G**) Phase of metabolites in the major oscillating metabolic classes. ***$P < 0.001$. All analyses were performed using $n = 4$ mice.

that were night fed (NF), i.e., food was available only in the mouse's active phase. An intact feeding-fasting cycle was sufficient for inducing ~52% of oscillating liver metabolites and 24% of oscillating liver transcripts, which are normally observed in WT mice (Fig. 4A), suggesting that the central clock and the feeding-fasting behavior affect on hepatic transcription to a similar degree. Further investigation of the transcriptome data identified gene sets with peak phases at the fasted (ZT4 to ZT8) and fed (ZT16 to ZT20) state in both brain-RE and KO NF mice (fig. S9A). These genes are suggested to be regulated by feeding-fasting rhythms independent of the presence of a central clock. Insights on the hepatic transcriptional integrators of feeding-fasting signals were assessed by a transcription factor enrichment analysis. The transcriptional fingerprint of the fasted state is suggested to be regulated by transcription factors responding to growth factors and oxidative stress (fig. S9B). Among these, Foxo3 was identified, which has been proposed to protect the circadian clock against oxidative stress (*33*). Furthermore, the fed state was characterized by a transcriptional program predicted to be mediated by transcription factors involved in circadian rhythms as well as lipid and carbohydrate metabolism (fig. S9C). The transcription factor Ppargc1a (PGC-1α) was identified at the core of the transcriptional interactome and is involved in all enriched biological processes among these transcription factors, suggesting that it is a key integrator of metabolic and circadian rhythms. This notion is supported by a previous work (*34*).

Strikingly, 56% of circulating metabolic rhythms were rescued in *Bmal1*-KO mice simply by establishing a feeding rhythm for them (table S3 and Fig. 4B). Further, ad libitum–fed brain-RE mice and NF-KO had almost an identical percent of recovery of the circadian metabolism and transcription of their respective WT littermates (Fig. 4C), showing that night feeding reinstated serum metabolite rhythms in KO mice to a level similar to that of brain-RE manipulation. The commonly oscillating metabolites between WT NF and KO NF were enriched for the acylcarnitine pathway (fig. S10A), in line with the shared pathways between brain-RE and WT mice. Nevertheless, the oscillating pattern of circulating metabolites in NF-KO and NF-WT mice was not identical to brain-RE or WT mice (fed ad libitum) (Fig. 4D): Although we observed a 4-hour delay in the early light-phase peak of the oscillating metabolites that were restored in brain-RE and KO NF, the uniquely rhythmic metabolites peaked in antiphase in the NF mice (Fig. 4E) and did not belong to the same pathways as in WT and brain-RE mice (fig. S10, B and C). In addition and in contrast to the higher amplitudes observed in brain-RE, the amplitude of the commonly oscillating metabolites was significantly lower in NF KO versus (ad libitum–fed) WT mice (Fig. 4F). Last, the same major metabolite classes displayed oscillations and peak times in NF-KO mice that were similar to those in WT and brain-RE mice, including a 4-hour delay in the lipid peak in relation to WT (Fig. 4G). In summary, these data suggest that the central clock regulates a significant proportion of peripheral metabolic rhythms likely via feeding-fasting behavior, yet other clocks are required for a fully functioning circadian rhythmicity and for controlling certain aspects of the peripheral metabolic response to feeding, such as amplitude and phase.

We are just starting to dissect the complex mechanisms governing circadian interorgan communication (*4*). Here, we show that the central clock is sufficient for driving systemic rhythms to a large extent via regulation of feeding-fasting rhythms. It is known that food is a major synchronizing factor that contributes to the role of the SCN as a master pacemaker (*35*). Moreover, the notion that the SCN synchronizes some peripheral clocks via factors in circulation is supported by parabiosis experiments (*36*). However, our data suggest that peripheral clocks not only are synchronized by food intake but buffer and integrate the metabolic rhythms. Recently, we demonstrated an integrative role for the autonomous liver clock in the presence of feeding-fasting cycles (*23*), revealing cooperation between the feeding-fasting cycles and the local clockwork in defining local rhythmic transcription. Supporting our findings, the hepatic clock has also been shown to shield untimely food intake and protect feeding-driven transcriptional rhythms in other peripheral tissues, such as the lung (*37*). It should be stressed that the phenotypes observed in brain-RE mice are independent of peripheral clocks; however, other neuronal clocks may explain some of the oscillations that are not restored (fig. S1C). In addition, it is possible that the de novo oscillating metabolites in the brain-RE and/or NF-KO mice drive aberrant rhythms in various tissues and thus require the liver clock to dampen their metabolic amplitude. Together, this work presents the central clock as a key driver of systemic metabolic rhythms; future studies will elucidate how these metabolic signals are interpreted by various peripheral clocks and how they can be best implemented into clinical therapies to treat morbidities associated to disrupted circadian rhythms (*38*).

METHODS

Animals

Mice were bred and housed in the animal facilities at the University of California, Irvine (UCI) vivarium and Barcelona Science Park, Spain, in accordance with the guidelines of the Institutional Animal Care and Use Committee at UCI and European Union and Spanish regulations, respectively. Animal experiments were designed and conducted with consideration of the ARRIVE (Animal Research: Reporting of In Vivo Experiments) guidelines, the details of which were as follows: Identical experimental conditions were in place at both institutions, and all mice were derived from the same founder line. *Bmal1*-stop-FL mice were generated as described previously (*9*, *10*). All experiments used 8- to 12-week-old male mice on a 12-hour light/12-hour dark cycle (or under constant darkness, for analyses of locomotor and indirect calorimetry) and fed ad libitum. Experimental mice were as follows: KO *Bmal1*$^{stopFL/stopFL}$, cre$^{-/-}$; liver-RE (LRE) *Bmal1*$^{stopFL/stopFL}$, *Alfp*-cre$^{-/tg}$; muscle-RE (MRE) *Bmal1*$^{stopFL/stopFL}$, *Hsa*-cre$^{-/tg}$; and brain-RE (BRE) *Bmal1*$^{stopFL/stopFL}$, *Syt10*-cre$^{-/tg}$. Metabolomics analyses in ad libitum–fed mice were performed using KO and WT littermates from all three genotypes: *Bmal1*$^{wt/wt}$, *Alfp*-cre$^{-/tg}$; *Bmal1*$^{wt/wt}$, *Hsa*-cre$^{-/tg}$; and *Bmal1*$^{wt/wt}$, *Syt10*-cre$^{-/tg}$. Metabolomics analyses in NF mice were performed in WT *Bmal1*$^{wt/wt}$, *Alfp*-cre$^{-/tg}$, and KO mice from the same colony. RNA-seq was performed using mice from the BRE colony, i.e., the *Bmal1*$^{wt/wt}$, *Syt10*-cre$^{-/tg}$ WTs. Mice were individually house for 2 weeks before euthanization and tissue harvest.

Global metabolomics analyses

Blood was collected from mice immediately after euthanization and stored on ice for ~30 min before centrifugation (3000 rpm for 10 min in 4°C). Serum was collected in a fresh tube, snap-frozen in liquid nitrogen, and stored in −80°C until shipment on dry ice to Metabolon Inc. Following receipt, samples were inventoried and immediately stored at −80°C. Each sample received was accessioned

into the Metabolon LIMS (Laboratory Information Management System) system and was assigned by the LIMS a unique identifier that was associated with the original source identifier only. This identifier was used to track all sample handling, tasks, results, etc.

Samples were prepared using the automated Microlab STAR system from Hamilton Company. Several recovery standards were added before the first step in the extraction process for quality control (QC) purposes. To remove the protein, dissociate small molecules bound to protein or trapped in the precipitated protein matrix and to recover chemically diverse metabolites, proteins were precipitated with methanol under vigorous shaking for 2 min (Glen Mills Geno/Grinder 2000) followed by centrifugation. The resulting extract was divided into five fractions: two for analysis by two separate reverse phase (RP)/ultraperformance LC (UPLC)–MS/MS methods with positive ion mode electrospray ionization (ESI), one for analysis by RP/UPLC-MS/MS with negative ion mode ESI, one for analysis by hydrophilic interaction liquid chromatography (HILIC)/UPLC-MS/MS with negative ion mode ESI, and one reserved as a backup. Samples were placed briefly on a TurboVap (Zymark) to remove the organic solvent. Sample extracts were stored overnight under nitrogen before preparation for analysis. Several types of controls were analyzed in concert with the experimental samples: a pooled matrix sample generated by taking a small volume of each experimental sample (or alternatively, use of a pool of well-characterized human plasma), as a technical replicate throughout the dataset; extracted water samples, as process blanks; and a cocktail of QC standards that were carefully chosen not to interfere with the measurement of endogenous compounds, which were spiked into every analyzed sample to allow instrument performance monitoring and to aid chromatographic alignment. Instrument variability was determined by calculating the median relative SD (RSD) for the standards that were added to each sample before injection into the mass spectrometers. The overall process variability was determined by calculating the median RSD for all endogenous metabolites (i.e., noninstrument standards) present in 100% of the pooled matrix samples. Experimental samples were randomized across the platform run with QC samples spaced evenly among the injections.

All methods used a Waters ACQUITY UPLC and a Thermo Scientific Q-Exactive high-resolution/accurate mass spectrometer interfaced with a heated ESI (HESI-II) source and Orbitrap mass analyzer operated at 35,000 mass resolution. The sample extract was dried and then reconstituted in solvents compatible to each of the four methods. Each reconstitution solvent contained a series of standards at fixed concentrations to ensure injection and chromatographic consistency. One aliquot was analyzed using acidic positive ion conditions and chromatographically optimized for more hydrophilic compounds. In this method, the extract was gradient eluted from a C18 column (Waters UPLC BEH C18, 2.1 mm by 100 mm, 1.7 μm) using water and methanol, containing 0.05% perfluoropentanoic acid (PFPA) and 0.1% formic acid (FA). Another aliquot was also analyzed using acidic positive ion conditions; however, it was chromatographically optimized for more hydrophobic compounds. In this method, the extract was gradient eluted from the same afore mentioned C18 column using methanol, acetonitrile, water, 0.05% PFPA, and 0.01% FA and was operated at an overall higher organic content. Another aliquot was analyzed using basic negative ion optimized conditions using a separate dedicated C18 column. The basic extracts were gradient eluted from the column using methanol and water but using 6.5 mM ammonium bicarbonate (pH 8). The fourth aliquot was analyzed via negative ionization following elution from a HILIC column (Waters UPLC BEH Amide, 2.1 mm by 150 mm, 1.7 μm) using a gradient consisting of water and acetonitrile with 10 mM ammonium formate (pH 10.8). The MS analysis alternated between MS and data-dependent MSn scans using dynamic exclusion. The scan range varied slighted between methods but covered mass-to-charge ratio (m/z) of 70 to 1000.

Raw data were extracted, peak-identified, and QC-processed using Metabolon's hardware and software. These systems are built on a web service platform using Microsoft's .NET technologies, which run on high-performance application servers and fiber-channel storage arrays in clusters to provide active failover and load balancing. Compounds were identified by comparison to library entries of purified standards or recurrent unknown entities. Metabolon maintains a library based on authenticated standards that contain the retention time/index (RI), m/z, and chromatographic data (including MS/MS spectral data) on all molecules present in the library. Furthermore, biochemical identifications are based on three criteria: retention index within a narrow RI window of the proposed identification, accurate mass match to the library ± 10 parts per million, and the MS/MS forward and reverse scores between the experimental data and authentic standards. The MS/MS scores are based on a comparison of the ions present in the experimental spectrum to the ions present in the library spectrum. While there may be similarities between these molecules based on one of these factors, the use of all three data points can be used to distinguish and differentiate biochemicals. More than 3300 commercially available, purified standard compounds have been acquired and registered into LIMS for analysis on all platforms for determination of their analytical characteristics. A variety of curation procedures was carried out to ensure that a high-quality dataset was available for statistical analysis and data interpretation. The QC and curation processes were designed to ensure accurate and consistent identification of true chemical entities and to remove those representing system artifacts, misassignments, and background noise. Metabolon data analysts use proprietary visualization and interpretation software to confirm the consistency of peak identification among the various samples. Library matches for each compound were checked for each sample and corrected if necessary.

Peaks were quantified using the area under the curve. A data normalization step was performed to correct variation resulting from instrument interday tuning differences. Essentially, each compound was corrected in run-day blocks by registering the medians to equal 1 and normalizing each data point proportionately. Furthermore, the data were normalized to the input volume of serum. Last, the results were analyzed, and clear outliers were excluded. Metabolic circadian rhythms were assessed using JTK_CYCLE (*12*), and P values < 0.05 were considered significant.

Indirect calorimetry and food intake

Indirect calorimetry was performed with negative flow Oxymax-CLAMS (Columbus Instruments, Columbus, OH) hardware system cages. Mice were given a 24-hour acclimation period to the metabolic cage. Measurements of energy expenditure, oxygen respiration (VO_2), carbon dioxide respiration (VCO_2), and food intake were taken every 10 min for two consecutive days after the 24-hour acclimation period at room temperature (RT). The respiratory exchange ratio (= VCO_2/VO_2) was calculated by the accompanying Oxymax software. The measurements were performed under 12-hour light/12-hour dark cycles or in constant darkness.

Locomotor activity

Locomotor activity of individually housed mice was measured using optical beam motion detection (Starr Life Sciences). Data were collected using Minimitter VitalView 5.0 data acquisition software and analyzed using Clocklab (Actimetrics). Mice were housed under 12-hour light/12-hour dark cycles for the initial 2 weeks, followed by a transition to 3 weeks in constant darkness.

Oral glucose tolerance test

Body weights were measured, and glucose (2 g kg^{-1}) was delivered orally. Blood glucose measurements were taken before injection and at 15, 30, 60, and 120 min after glucose injection at ZT14 using a Accu-Chek Aviva glucose meter kit. The specific time point was selected on the basis of previous work demonstrating that the necessity of the central clock for normal glucose tolerance was most important at ZT12 to ZT14 (*30*).

Protein extraction and Western blot

Frozen tissue pieces were placed in 1.5-ml Eppendorf tubes with radioimmunoprecipitation assay buffer [50 mM tris-HCl (pH 8.0), 150 mM NaCl, 1% NP-40, 0.5% sodium deoxycholate, 0.1% SDS, 5 mM $MgCl_2$, and 1 mM phenylmethylsulfonyl fluoride] supplemented with Protease Inhibitor Cocktail (Roche), 1 mM dithiothreitol, 20 mM NaF, 10 mM nicotinamide, and 330 nM trichostatin A (Sigma-Aldrich, T8552). Samples were homogenized using a VWR 200 homogenizer followed by a 10-s sonication at 60%. Tissue lysates were centrifugated at 13,200 rpm for 15 min at 4°C. Supernatants were transferred to a fresh tube, and an aliquot was used for protein quantification using the Bradford assay (Bio-Rad). A total of 10 to 20 μg of protein lysates were separated on 8% gels by SDS–polyacrylamide gel electrophoresis and transferred to nitrocellulose membranes. Membranes were incubated with primary anti-BMAL1 (Abcam, ab93806) and anti-P84 (GeneTex, GTX70220) antibodies overnight at 4°C and with peroxidase-conjugated secondary antibodies [anti-mouse immunoglobulin G (IgG), horseradish peroxidase (HRP) conjugate, EMD Millipore, AP160P; anti-rabbit IgG, HRP-linked, EMD Millipore, 12-348] for 1 hour at RT. Protein bands were visualized by chemiluminescent HRP substrate (EMD Millipore, WBKLS0500). Blots were developed with autoradiography films (HyBlot CL, Denville Scientific) or ChemiDoc MP Imaging System (Bio-Rad Laboratories).

Immunohistochemistry

Mouse brains were frozen at −80°C isopentane and sectioned in 10-μm-thick sections using Leica CM1950 Cryostat. Sections were fixed with ice-cold 4% paraformaldehyde for 20 min and washed three times with 1× phosphate-buffered saline (PBS). Samples were then permeabilized (1× PBS and 0.3% Triton X-100) for 15 min at RT, blocked (in 1× PBS, 5% bovine serum albumin, and 10% normal goat serum) for 2 hours at RT, and then incubated with a BMAL1 antibody (Novus, NB100-2288) diluted in a blocking buffer overnight at 4°C. Samples were washed three times with 1× PBS and incubated with Alexa Fluor 488 goat anti-rabbit IgG (Invitrogen, A-11008) for 2 hours at RT. After three washes with 1× PBS, nuclei were stained using DRAQ7 (BioStatus) for 15 min at RT and subsequently washed twice with 1× PBS.

RNA extraction and RNA-seq and analysis

Total RNA was extracted from liver with TRIzol (Invitrogen) and then precipitated with isopropanol and ethanol. Total RNA was monitored for QC using the Agilent Bioanalyzer Nano RNA chip and NanoDrop absorbance ratios for 260/280 nm and 260/230 nm. Libraries were constructed according to the Illumina TruSeq Stranded mRNA Sample Preparation Guide. The input quantity for total RNA was 1000 ng, and mRNA was enriched using oligo(dT) magnetic beads. The enriched mRNA was chemically fragmented for 3 min. The first-strand synthesis used random primers and reverse transcriptase to make complementary DNA (cDNA). After the second-strand synthesis, the double-stranded (ds)-cDNA was cleaned using AMPure XP beads, cDNA was end-repaired, and the 3′ ends were adenylated. Illumina barcoded adapters were ligated on the ends, and the adapter-ligated fragments were enriched by nine cycles of polymerase chain reaction (PCR). The resulting libraries were validated by quantitative PCR and sized using a Agilent Bioanalyzer DNA high-sensitivity chip. The concentrations for the libraries were normalized and then multiplexed together. The multiplexed libraries were sequenced on paired-end 100-cycle chemistry on the NovaSeq 6000. The NovaSeq control software NVCS version 1.7.0 was used with real-time analysis software, RTA 3.4.4.

Reads from each replicate experiment were aligned to the reference genome assembly mm10 and to the corresponding transcriptome using TopHat. Subsequently, gene expression levels were computed from the read alignment results using Cufflinks, another tool in the Tuxedo protocol. This protocol outputs the FPKM (fragments per kilobase of transcript per million mapped reads) values for each gene of each replicate. To determine the periodicity of genes, the JTK_CYCLE (*12*) algorithm was used, and data were validated using the BIO_CYCLE algorithm (*39*). All analyses were robustly consistent across both methods. The output of these algorithms includes the amplitude, phase, and *P* value for each transcript. Genes were considered circadian if their *P* value output by JTK_CYCLE was <0.01. Heatmaps of circadian transcripts were generated using the R package gplots v3.0.3, in which the rows are sorted by the JTK_CYCLE output phase and row *z*-score normalized. Gene ontology, pathway, and transcription factor analyses were performed using ToppFun (https://toppgene.cchmc.org/). Protein interactomes and gene ontology within the interactomes were performed using STRING: functional protein association networks (string-db.org).

Statistics

For each experiment, the number of biological replicates, statistical test, significance threshold, and visual representation information (i.e., mean and SEM of graphs) are given in the figure legends.

SUPPLEMENTARY MATERIALS

Supplementary material for this article is available at https://science.org/doi/10.1126/sciadv.abo2896

View/request a protocol for this paper from *Bio-protocol*.

REFERENCES AND NOTES

1. J. S. Takahashi, Transcriptional architecture of the mammalian circadian clock. *Nat. Rev. Genet.* **18**, 164–179 (2017).
2. K. B. Koronowski, P. Sassone-Corsi, Communicating clocks shape circadian homeostasis. *Science* **371**, eabd0951 (2021).
3. J. Ye, R. Medzhitov, Control strategies in systemic metabolism. *Nat. Metab.* **1**, 947–957 (2019).
4. H. Reinke, G. Asher, Crosstalk between metabolism and circadian clocks. *Nat. Rev. Mol. Cell Biol.* **20**, 227–241 (2019).
5. K. A. Dyar, D. Lutter, A. Artati, N. J. Ceglia, Y. Liu, D. Armenta, M. Jastroch, S. Schneider, S. de Mateo, M. Cervantes, S. Abbondante, P. Tognini, R. Orozco-Solis, K. Kinouchi, C. Wang, R. Swerdloff, S. Nadeef, S. Masri, P. Magistretti, V. Orlando, E. Borrelli, N. H. Uhlenhaut, P. Baldi, J. Adamski, M. H. Tschöp, K. Eckel-Mahan, P. Sassone-Corsi, Atlas

of circadian metabolism reveals system-wide coordination and communication between clocks. *Cell* **174**, 1571–1585.e11 (2018).
6. P. L. Lowrey, J. S. Takahashi, in *Advances in Genetics* (Academic Press Inc., 2011), vol. 74, pp. 175–230.
7. J. Bass, J. S. Takahashi, Circadian integration of metabolism and energetics. *Science* **330**, 1349–1354 (2010).
8. S. Panda, Circadian physiology of metabolism. *Science* **354**, 1008–1015 (2016).
9. K. B. Koronowski, K. Kinouchi, P.-S. Welz, J. G. Smith, V. M. Zinna, J. Shi, M. Samad, S. Chen, C. N. Magnan, J. M. Kinchen, W. Li, P. Baldi, S. A. Benitah, P. Sassone-Corsi, Defining the independence of the liver circadian clock. *Cell* **177**, 1448–1462.e14 (2019).
10. P.-S. Welz, V. M. Zinna, A. Symeonidi, K. B. Koronowski, K. Kinouchi, J. G. Smith, I. M. Guillén, A. Castellanos, S. Furrow, F. Aragón, G. Crainiciuc, N. Prats, J. M. Caballero, A. Hidalgo, P. Sassone-Corsi, S. A. Benitah, BMAL1-driven tissue clocks respond independently to light to maintain homeostasis. *Cell* **177**, 1436–1447.e12 (2019).
11. J. G. Smith, K. B. Koronowski, T. Sato, C. Greco, P. Petrus, A. Verlande, S. Chen, M. Samad, E. Deyneka, L. Mathur, R. Blazev, J. Molendijk, T. Mortimer, A. Kumar, O. Deryagin, M. Vaca-Dempere, P. Liu, V. Orlando, B. L. Parker, P. Baldi, P.-S. Welz, C. Jang, S. Masri, S. A. Benitah, P. Muñoz-Cánoves, P. Sassone-Corsi, Interrogating metabolic interactions between skeletal muscle and liver circadian clocks in vivo. bioRxiv 482160 (2022); https://doi.org/10.1101/2022.02.27.482160.
12. M. E. Hughes, J. B. Hogenesch, K. Kornacker, JTK_CYCLE: An efficient nonparametric algorithm for detecting rhythmic components in genome-scale data sets. *J. Biol. Rhythms* **25**, 372–380 (2010).
13. Y. Nakahata, S. Sahar, G. Astarita, M. Kaluzova, P. Sassone-Corsi, Circadian control of the NAD^+ salvage pathway by CLOCK-SIRT1. *Science* **324**, 654–657 (2009).
14. Y. Nakahata, M. Kaluzova, B. Grimaldi, S. Sahar, J. Hirayama, D. Chen, L. P. Guarente, P. Sassone-Corsi, The NAD+-dependent deacetylase SIRT1 modulates CLOCK-mediated chromatin remodeling and circadian control. *Cell* **134**, 329–340 (2008).
15. H. Abe, S. Honma, H. Ohtsu, K. I. Honma, Circadian rhythms in behavior and clock gene expressions in the brain of mice lacking histidine decarboxylase. *Brain Res. Mol. Brain Res.* **124**, 178–187 (2004).
16. K. A. Dyar, M. J. Hubert, A. A. Mir, S. Ciciliot, D. Lutter, F. Greulich, F. Quagliarini, M. Kleinert, K. Fischer, T. O. Eichmann, L. E. Wright, M. I. Peña Paz, A. Casarin, V. Pertegato, V. Romanello, M. Albiero, S. Mazzucco, R. Rizzuto, L. Salviati, G. Biolo, B. Blaauw, S. Schiaffino, N. H. Uhlenhaut, Transcriptional programming of lipid and amino acid metabolism by the skeletal muscle circadian clock. *PLOS Biol.* **16**, e2005886 (2018).
17. D. R. Weaver, The suprachiasmatic nucleus: A 25-year retrospective. *J. Biol. Rhythms* **13**, 100–112 (1998).
18. E. S. Lein, M. J. Hawrylycz, N. Ao, M. Ayres, A. Bensinger, A. Bernard, A. F. Boe, M. S. Boguski, K. S. Brockway, E. J. Byrnes, L. Chen, L. Chen, T.-M. Chen, M. C. Chin, J. Chong, B. E. Crook, A. Czaplinska, C. N. Dang, S. Datta, N. R. Dee, A. L. Desaki, T. Desta, E. Diep, T. A. Dolbeare, M. J. Donelan, H.-W. Dong, J. G. Dougherty, B. J. Duncan, A. J. Ebbert, G. Eichele, L. K. Estin, C. Faber, B. A. Facer, R. Fields, S. R. Fischer, T. P. Fliss, C. Frensley, S. N. Gates, K. J. Glattfelder, K. R. Halverson, M. R. Hart, J. G. Hohmann, M. P. Howell, D. P. Jeung, R. A. Johnson, P. T. Karr, R. Kawal, J. M. Kidney, R. H. Knapik, C. L. Kuan, J. H. Lake, A. R. Laramee, K. D. Larsen, C. Lau, T. A. Lemon, A. J. Liang, Y. Liu, L. T. Luong, J. Michaels, J. J. Morgan, R. J. Morgan, M. T. Mortrud, N. F. Mosqueda, L. L. Ng, R. Ng, G. J. Orta, C. C. Overly, T. H. Pak, S. E. Parry, S. D. Pathak, O. C. Pearson, R. B. Puchalski, Z. L. Riley, H. R. Rockett, S. A. Rowland, J. J. Royall, M. J. Ruiz, N. R. Sarno, K. Schaffnit, N. V. Shapovalova, T. Sivisay, C. R. Slaughterbeck, S. C. Smith, K. A. Smith, B. I. Smith, A. J. Sodt, N. N. Stewart, K. R. Stumpf, S. M. Sunkin, M. Sutram, A. Tam, C. D. Teemer, C. Thaller, C. L. Thompson, L. R. Varnam, A. Visel, R. M. Whitlock, P. E. Wohnoutka, C. K. Wolkey, V. Y. Wong, M. Wood, M. B. Yaylaoglu, R. C. Young, B. L. Youngstrom, X. F. Yuan, B. Zhang, T. A. Zwingman, A. R. Jones, Genome-wide atlas of gene expression in the adult mouse brain. *Nature* **445**, 168–176 (2007).
19. J. Husse, X. Zhou, A. Shostak, H. Oster, G. Eichele, Synaptotagmin10-Cre, a driver to disrupt clock genes in the SCN. *J. Biol. Rhythms* **26**, 379–389 (2011).
20. K. A. Dyar, S. Ciciliot, L. E. Wright, R. S. Biensø, G. M. Tagliazucchi, V. R. Patel, M. Forcato, M. I. P. Paz, A. Gudiksen, F. Solagna, M. Albiero, I. Moretti, K. L. Eckel-Mahan, P. Baldi, P. Sassone-Corsi, R. Rizzuto, S. Bicciato, H. Pilegaard, B. Blaauw, S. Schiaffino, Muscle insulin sensitivity and glucose metabolism are controlled by the intrinsic muscle clock. *Mol. Metab.* **3**, 29–41 (2014).
21. K. A. Lamia, K. F. Storch, C. J. Weitz, Physiological significance of a peripheral tissue circadian clock. *Proc. Natl. Acad. Sci. U.S.A.* **105**, 15172–15177 (2008).
22. R. Lin, Y. Mo, H. Zha, Z. Qu, P. Xie, Z.-J. Zhue, Y. Xu, Y. Xiong, K.-L. Guan, CLOCK acetylates ASS1 to drive circadian rhythm of ureagenesis. *Mol. Cell* **68**, 198–209.e6 (2017).
23. C. M. Greco, K. B. Koronowski, J. G. Smith, J. Shi, P. Kunderfranco, R. Carriero, S. Chen, M. Samad, P.-S. Welz, V. M. Zinna, T. Mortimer, S. K. Chun, K. Shimaji, T. Sato, P. Petrus, A. Kumar, M. Vaca-Dempere, O. Deryagian, C. Van, J. M. M. Kuhn, D. Lutter, M. M. Seldin, S. Masri, W. Li, P. Baldi, K. A. Dyar, P. Muñoz-Cánoves, S. A. Benitah, P. Sassone-Corsi, Integration of feeding behavior by the liver circadian clock reveals network dependency of metabolic rhythms. *Sci. Adv.* **7**, eabi7828 (2021).
24. B. Kornmann, O. Schaad, H. Bujard, J. S. Takahashi, U. Schibler, System-driven and oscillator-dependent circadian transcription in mice with a conditionally active liver clock. *PLOS Biol.* **5**, e34 (2007).
25. B. Grimaldi, M. M. Bellet, S. Katada, G. Astarita, J. Hirayama, R. H. Amin, J. G. Granneman, D. Piomelli, T. Leff, P. Sassone-Corsi, PER2 controls lipid metabolism by direct regulation of PPARγ. *Cell Metab.* **12**, 509–520 (2010).
26. C. B. Peek, D. C. Levine, J. Cedernaes, A. Taguchi, Y. Kobayashi, S. J. Tsai, N. A. Bonar, M. R. McNulty, K. M. Ramsey, J. Bass, Circadian clock interaction with HIF1α mediates oxygenic metabolism and anaerobic glycolysis in skeletal muscle. *Cell Metab.* **25**, 86–92 (2017).
27. R. G. Carroll, G. A. Timmons, M. P. Cervantes-Silva, O. D. Kennedy, A. M. Curtis, Immunometabolism around the clock. *Trends Mol. Med.* **25**, 612–625 (2019).
28. C. M. Greco, M. Cervantes, J.-M. Fustin, K. Ito, N. Ceglia, M. Samad, J. Shi, K. B. Koronowski, I. Forne, S. Ranjit, J. Gaucher, K. Kinouchi, R. Kojima, E. Gratton, W. Li, P. Baldi, A. Imhof, H. Okamura, P. Sassone-Corsi, S-adenosyl-L-homocysteine hydrolase links methionine metabolism to the circadian clock and chromatin remodeling. *Sci. Adv.* **6**, eabc5629 (2020).
29. M. G. Schooneman, F. M. Vaz, S. M. Houten, M. R. Soeters, Acylcarnitines: Reflecting or inflicting insulin resistance? *Diabetes* **62**, 1–8 (2013).
30. G. Ding, X. Li, X. Hou, W. Zhou, Y. Gong, F. Liu, Y. He, J. Song, J. Wang, P. Basil, W. Li, S. Qian, P. Saha, J. Wang, C. Cui, T. Yang, K. Zou, Y. Han, C. I. Amos, Y. Xu, L. Chen, Z. Sun, REV-ERB in GABAergic neurons controls diurnal hepatic insulin sensitivity. *Nature* **592**, 763–767 (2021).
31. A. Chaix, T. Lin, H. D. Le, M. W. Chang, S. Panda, Time-restricted feeding prevents obesity and metabolic syndrome in mice lacking a circadian clock. *Cell Metab.* **29**, 303–319.e4 (2019).
32. J. Qian, F. A. J. L. Scheer, Circadian system and glucose metabolism: Implications for physiology and disease. *Trends Endocrinol. Metab.* **27**, 282–293 (2016).
33. X. Zheng, Z. Yang, Z. Yue, J. D. Alvarez, A. Sehgal, FOXO and insulin signaling regulate sensitivity of the circadian clock to oxidative stress. *Proc. Natl. Acad. Sci. U.S.A.* **104**, 15899–15904 (2007).
34. C. Liu, S. Li, T. Liu, J. Borjigin, J. D. Lin, Transcriptional coactivator PGC-1α integrates the mammalian clock and energy metabolism. *Nature* **447**, 477–481 (2007).
35. G. Asher, P. Sassone-Corsi, Time for food: The intimate interplay between nutrition, metabolism, and the circadian clock. *Cell* **161**, 84–92 (2015).
36. H. Guo, J. M. K. Brewer, A. Champhekar, R. B. S. Harris, E. L. Bittman, Differential control of peripheral circadian rhythms by suprachiasmatic-dependent neural signals. *Proc. Natl. Acad. Sci. U.S.A.* **102**, 3111–3116 (2005).
37. G. Manella, E. Sabath, R. Aviram, V. Dandavate, S. Ezagouri, M. Golik, Y. Adamovich, G. Asher, The liver-clock coordinates rhythmicity of peripheral tissues in response to feeding. *Nat. Metab.* **3**, 829–842 (2021).
38. C. R. Cederroth, U. Albrecht, J. Bass, S. A. Brown, J. Dyhrfjeld-Johnsen, F. Gachon, C. B. Green, M. H. Hastings, C. Helfrich-Förster, J. B. Hogenesch, F. Lévi, A. Loudon, G. B. Lundkvist, J. H. Meijer, M. Rosbash, J. S. Takahashi, M. Young, B. Canlon, Medicine in the fourth dimension. *Cell Metab.* **30**, 238–250 (2019).
39. F. Agostinelli, N. Ceglia, B. Shahbaba, P. Sassone-Corsi, P. Baldi, What time is it? Deep learning approaches for circadian rhythms. *Bioinformatics* **32**, i8–i17 (2016).
40. N. Ceglia, Y. Liu, S. Chen, F. Agostinelli, K. Eckel-Mahan, P. Sassone-Corsi, P. Baldi, CircadiOmics: Circadian omic web portal. *Nucleic Acids Res.* **46**, W157–W162 (2018).
41. V. R. Patel, K. Eckel-Mahan, P. Sassone-Corsi, P. Baldi, CircadiOmics: Integrating circadian genomics, transcriptomics, proteomics and metabolomics. *Nat. Methods* **9**, 772–773 (2012).

Acknowledgment: We thank all members of the Sassone-Corsi laboratory for helpful discussion and technical assistance. We appreciate M. Oakes and S.-A. Chung at the UCI Genomics High-Throughput Facility. Furthermore, we thank the committee consisting of faculty in the Department of Biological Chemistry and the Department of Microbiology and Molecular Genetics at UCI for support after the passing of P.S.-C. We thank V. Raker for manuscript editing. **Funding:** P.P. was funded by the Wenner-Gren Foundation; the Foundation Blanceflor Boncompagni Ludovisi, née Bildt; and the Tore Nilsson Foundation for Medical Science. Funding for P.S.-C. was provided by the National Institutes of Health (NIH) (AG053592 and DK114652), a Novo Nordisk Foundation Challenge Grant, and Institut National de la Sante et la Recherche Medicale (U1233 INSERM, France). Research in the S.A.B. laboratory is supported partially by the European Research Council (ERC) under the European Union's Horizon 2020 research and innovation programme (grant agreement no. 787041), the Government of Cataluña (SGR grant), the Government of Spain (MINECO), the La Marató/TV3 Foundation, the Foundation Lilliane Bettencourt, the Spanish Association for Cancer Research (AECC), and the Worldwide Cancer Research Foundation (WCRF). The IRB Barcelona is a Severo Ochoa Center of Excellence (MINECO award SEV-2015-0505). P.M.C. acknowledges funding from

MICINN-RTI2018-096068, ERC-2016-AdG-741966, LaCaixa-HEALTH-HR17-00040, MDA, UPGRADE-H2020-825825, AFM, DPP-Spain, Fundació La Marató TV3-80/19-202021, MWRF, María-de-Maeztu Program for Units of Excellence to UPF (MDM-2014-0370), and the Severo- Ochoa Program for Centers of Excellence to CNIC (SEV-2015-0505). T.S. was supported by a Japan Society for the Promotion of Science (JSPS) fellowship. C.M.G. was funded by European Union's Horizon 2020 research and innovation programme under the Marie Skłodowska-Curie grant agreement no. 749869. T.M. received funding from the European Union's Horizon 2020 research and innovation programme under the Marie Skłodowska-Curie grant agreement no. 754510. P.-S.W. is supported by grant RYC2019-026661-I funded by MCIN/AEI/10.13039/501100011033 and by "ESF Investing in your future." We acknowledge predoctoral fellowships to M.C. from the NIH (GM117942), the American Heart Association (17PRE33410952), and the UCI School of Medicine Behrens Research Excellence Award. The work of S.C. and P.B. was, in part, supported by NIH grant NIH GM123558. **Author contributions:** P.P., J.G.S., K.B.K., P.M.-C., P. S.-C., and S.A.B. designed the study and analyzed the data. P.P., J.G.S., K.B.K., T.S., C.M.G., T.M., P.-S.W., V.M.Z., K.S., M.C., and D.P. performed experiments and/or interpreted the results. S.C. and P.B. performed the bioinformatics analyses. P.P. wrote the first version of the paper with feedback from all authors. **Competing interests:** The authors declare that they have no competing interests. **Data and materials availability:** All data needed to evaluate the conclusions in the paper are present in the paper or the Supplementary Materials. The metabolomics and transcriptomics data and its analyses are available from the CircadiOmics web portal (*40*, *41*), where both JTK_CYCLE and BIO_CYCLE parameters are available. The transcriptomics data are also available through the Gene Expression Omnibus repository (GSE196430).

Submitted 25 January 2022
Accepted 9 May 2022
Published 29 June 2022
10.1126/sciadv.abo2896